GEOLOGY

Explosive-effusive volcanic eruption transitions caused by sintering

Fabian B. Wadsworth[1]*, Edward W. Llewellin[1], Jérémie Vasseur[2], James E. Gardner[3], Hugh Tuffen[4]

Silicic volcanic activity has long been framed as either violently explosive or gently effusive. However, recent observations demonstrate that explosive and effusive behavior can occur simultaneously. Here, we propose that rhyolitic magma feeding subaerial eruptions generally fragments during ascent through the upper crust and that effusive eruptions result from conduit blockage and sintering of the pyroclastic products of deeper cryptic fragmentation. Our proposal is supported by (i) rhyolitic lavas are volatile depleted; (ii) textural evidence supports a pyroclastic origin for effusive products; (iii) numerical models show that small ash particles $\lesssim 10^{-5}$ m can diffusively degas, stick, and sinter to low porosity, in the time available between fragmentation and the surface; and (iv) inferred ascent rates from both explosive and apparently effusive eruptions can overlap. Our model reconciles previously paradoxical observations and offers a new framework in which to evaluate physical, numerical, and geochemical models of Earth's most violent volcanic eruptions.

INTRODUCTION

Direct observations of eruptive behavior from Volcán Chaitén in 2008 (*1*) and Cordón Caulle in 2011 and 2012 (*2*) revealed that effusion of lava can be coincident with either sustained or intermittent explosive behavior: Gas and ash were discharged explosively from fractures within effusing lavas that filled the vent. These observations overturned the paradigm that silicic eruptions must necessarily be either violently explosive, producing ash-rich plumes that may encircle the globe and affect Earth's climate (*3*) or effusive, producing lava flows locally at the vent (*4*). Understanding the controls on eruption style is a grand challenge of modern geoscience (*5*) because it is key to forecasting the evolution of the resultant volcanic hazard.

During the 2008 eruption of Volcán Chaitén, seismicity associated with brittle magma failure (*6*) continued after the Plinian explosive phase, through the hybrid effusive-explosive phase and into the effusive phase (*7*). These findings are at odds with conventional conceptions of eruptive style transitions. Here, we propose a model that is consistent with available evidence and encompasses wide-ranging data and observations. In the framework of our model, explosive fragmentation of the magma may persist through all stages of a rhyolite eruption—explosive, hybrid, and effusive. Effusive lavas are the sintered products of volcanic ash and pyroclasts, and variations in style are a function of variable occlusion of the conduit by lava.

Foam or fracture outgassing?

In the crustal magma reservoir, rhyolite contains dissolved water, and magma ascent is driven by the growth of bubbles of gas that form when the water comes out of solution (*8*, *9*). However, the initial water content of the magma is similar across all eruption styles [Fig. 1A; data from glass inclusion studies from 7 volcanoes (*10*–*12*)], indicating that initial water content does not determine whether magma erupts explosively or effusively. By contrast, the water content that remains dissolved in the erupted products (pumice, ash, or lava) is substantially lower for effusive eruptions than for explosive eruptions [Fig. 1B; data from 14 volcanoes (*10*, *12*–*19*)]. The products of hybrid eruptions (*2*, *18*)—those that simultaneously display both effusive and explosive characteristics—straddle the effusive and explosive fields. Counterintuitively, explosive products are dominated by high-porosity pumice, demonstrating abundant degassing into bubbles, whereas effusive products are dominated by low-porosity lava with little direct evidence of bubble growth. A general model for the formation of effusive and explosive eruption products must therefore explain how the same magma, with initially high water content, can produce variably degassed high-porosity pumice and highly degassed low-porosity lava.

Previous models fall into two broad schools of thought. The first supports a permeable foam model, which contends that bubbles and pore space in the ascending magma connect to form a permeable network through which magmatic gas escapes, allowing the foam to collapse to produce a dense, degassed lava (*8*, *20*, *21*). However, densification of foams by collapse is a self-limiting process because permeability becomes negligible below 20 to 30 volume % (vol %) porosity (*22*, *23*), preventing further gas escape. Even where magmatic foams are sheared, which enhances permeability even at lower porosities, the lowest porosity achieved experimentally (*24*) is 17 vol %, whereas natural glassy lavas commonly have porosity below 5 vol % (*20*). In the permeable foam paradigm, such low porosities require that lavas ubiquitously undergo repressurization to resorb bubbles (*21*), yet there is no independent evidence to support this conjecture. If repressurization was the mechanism by which porosity was reduced to observed values, then diffusion of volatiles back into the melt would have occurred, and the glass preserved in effusive lavas at Earth's surface would not have such low dissolved water concentrations (Fig. 1) (*21*).

The second school of thought supports a fracture degassing model, which contends that the viscoelastic magma fractures repetitively as a result of high local strain rates at the margins of the conduit (*9*), allowing gas to escape through a transient fracture network; the fractures then seal and heal to form a dense, degassed lava (*17*, *18*, *25*). This model requires very close fracture spacing (interfracture

[1]Department of Earth Sciences, Durham University, Science Labs, Durham DH1 3LE, UK. [2]Earth and Environmental Sciences, Ludwig-Maximilians-Universität, Theresienstr. 41, 80333 Munich, Germany. [3]Department of Geological Sciences, Jackson School of Geosciences, The University of Texas at Austin, 2305 Speedway Stop C1160, Austin, TX 78712-1692, USA. [4]Lancaster Environment Centre, Lancaster University, Lancaster LA1 4YQ, UK.
*Corresponding author. Email: fabian.b.wadsworth@durham.ac.uk

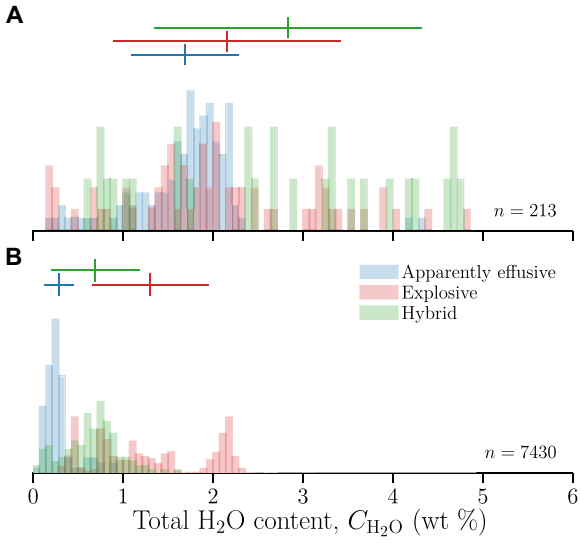

Fig. 1. The water content of erupted rhyolites worldwide. (**A**) The distribution of dissolved water measured in glass inclusions trapped in crystals for a range of rhyolite eruptions (213 data points) (*10*–*12*). Taken to represent the initial, dominant volatile conditions for ascent, these values are similar in variance and mean value and do not vary substantially with eruptive style (we do not account for volatile loss after entrapment). (**B**) The distribution of dissolved total water content remaining in the groundmass glass of eruptive products, in a second global database of rhyolite compositions compiled here (7430 data points) (*10*, *12*–*19*, *46*). Effusive eruption products have substantially lower water than explosive products; hybrid products fill the gap, forming a continuum. wt % is used to denote weight %.

distances as low as 10^{-5} to 10^{-4} m) to explain measured low volatile concentrations in rhyolite lavas (*17*), but evidence for pervasive, closely spaced fractures in lavas is not always found (*17*, *26*). Some fracture-degassing models allow for the shear-induced failure of melt in a conduit-margin annulus (*9*), allowing this region to degas efficiently before sintering and healing to form dense lava. However, this leaves the larger conduit core magma (>76% of the volume; see Materials and Methods) to outgas by other means. Neither the permeable foam nor the fracture degassing model can thus fully explain the vesicle- and volatile-poor nature of rhyolitic obsidian lavas.

RESULTS

Cryptic fragmentation

We propose a conceptual model for the origin of effusive, explosive, and hybrid rhyolitic volcanism, in which effusive lavas are produced by sintering, in the shallow conduit, of the fragmentary products of deeper, cryptic fragmentation (Fig. 2). We start from the observation that the majority of studied silicic eruptions began with an explosive event (*5*) and evolved toward hybrid then effusive eruption styles (*2*). During the subaerially explosive phase, the volcanic conduit is filled, above the fragmentation level, with a turbulent, high-velocity dispersion of hot gas and fragmented blebs of high-viscosity magma (Fig. 2A). We propose that a proportion of these fragments stick to the conduit walls, where they sinter to form a low-porosity magma and are variably emplaced and removed in cycles of sticking and erosion (Fig. 2, B and C). As eruption rates wane, aggradation of sintered fragments dominates over erosion [c.f. (*27*)]. When sufficient sintered magma aggrades in the shallow conduit, it may extrude as lava, initially alongside, and subordinate to, the explosive products of continued deep fragmentation (Fig. 2C), but then as the primary eruptive product, as the shallow conduit becomes increasingly plugged (Fig. 2D). Total occlusion of the conduit may suppress fragmentation entirely, ultimately terminating the eruption.

There is abundant textural evidence in support of this cryptic fragmentation model. Evidence for wholesale fragmentation followed by sticking and welding of tephra to the walls of the conduit is preserved in glassy fragments that are subsequently ripped out and erupted with the explosive products (Fig. 2E) (*19*); these fragments show evidence for repeated welding and remobilization over a wide range of depths in the conduit (*19*). Hybrid activity that follows on from purely explosive eruptions of rhyolite is dominated by fractures opening through an extruding lava (*2*), which transiently connect the gas-fragment dispersion to the surface, feeding pulsatory explosive activity. The transport of the gas-fragment mixture through fractures is recorded by tuffisite veins within bombs that have been ejected from the vent before sintering completely (*17*, *25*, *28*) (Fig. 2F) or which are preserved in older, eroded conduit interiors (*29*). Tuffisites that intrude country rock adjacent to the conduit may constitute a sink for pressurized gas beneath the forming plug (*30*). Last, evidence for the sintering of fine-grained ash within apparently effusive rhyolite lava is provided by the 2011–2012 eruption of Cordón Caulle and older eruptions of the Mono Craters, United States (*31*). The walls of open fractures, preserved directly over the vents (Fig. 2G), are plastered with partially sintered, fine-grained glassy ash particles, representing a snapshot of the process we invoke, operating at the shallowest possible level.

In-conduit outgassing, sticking, and welding of particles

Any convincing validation of the cryptic fragmentation model should pass three simple quantitative tests of feasibility. First, in the time and space available between magma fragmentation and Earth's surface, the fragments that will sinter must be able to outgas to produce the observed low water content of rhyolite lavas. Second, conditions must be right for the fragments to stick to the walls of the conduit. Third, the captured fragments must be able to sinter to produce low-porosity lava that can then be extruded. We address each of these in turn.

First, we use a one-dimensional steady-state numerical eruption model (*32*) to assess conduit conditions during the explosive phase of a typical rhyolitic eruption, based on initial conditions for the well-studied 2008 eruption of Volcán Chaitén. We determine the depth of fragmentation, the concentration of dissolved water in the magma at fragmentation, and the pressure and velocity in the gas-fragment dispersion above fragmentation, as functions of depth (Fig. 3A). We use these parameters as inputs to a one-dimensional diffusion model, which calculates the residual water content of the fragments of magma as they ascend the conduit (see Materials and Methods and Fig. 3, B and C). We find that fragments with radius $R \lesssim 10^{-5}$ m can degas, during transport, to water contents consistent with those preserved in rhyolite lavas worldwide (Fig. 3D). This size, which is in the fine ash range of explosive eruptions (*31*), is consistent with particles observed to have sintered in natural obsidian pyroclasts (*19*) and lavas (Fig. 2G). The numerical eruption model does not capture the complex feedbacks among eruption rate, fragmentation depth, and pressure distribution that are anticipated as conduit occlusion progresses. However, since occlusion is likely to reduce eruption rate, leaving more time for outgassing, the model is a conservative test: Even under conditions typical of sustained explosive eruption, particles can outgas during transport from fragmentation to vent.

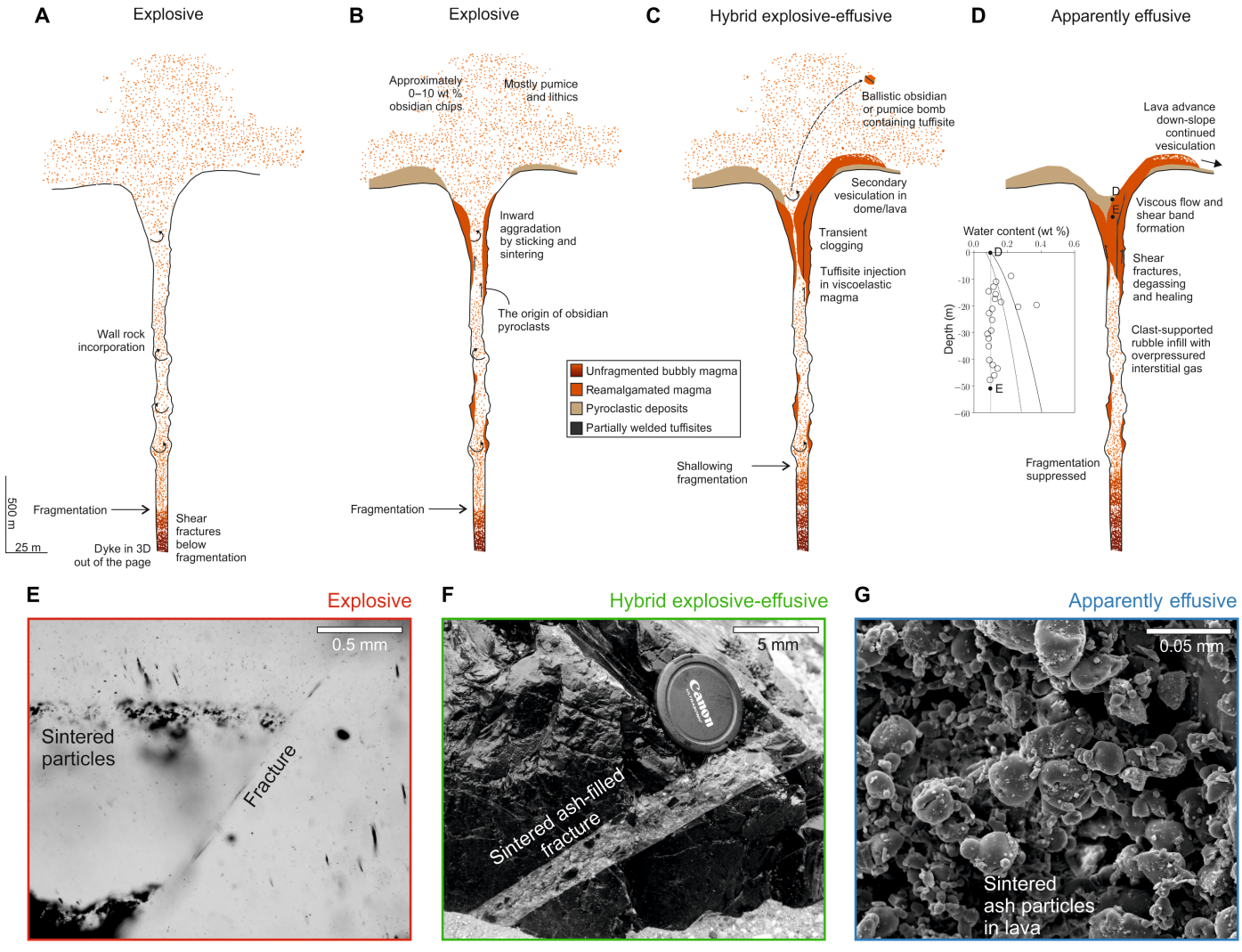

Fig. 2. A new cryptic fragmentation model to explain the textural and chemical record of rhyolitic volcanism. (**A** to **D**) Schematic summaries of the cryptic fragmentation model for rhyolitic volcanism. We note that this schematic is necessarily a simplification of what may be a more complex three-dimensional (3D) picture. Hydrostatic considerations indicate that a pressure of just a few megapascals at the base of the aggrading mass (in C and D) is sufficient to drive effusion. Inset in (D) shows data for H_2O from the shallow drilling of the Obsidian Dome (*20*), showing that shallowest apparently effusive eruptions are equilibrated below magmastatic conditions, at an approximate atmospheric pressure down to −50 m below the surface, a feature consistent with our model. (**E** to **G**) The textural record of fragmentation and welding in rhyolites. (E) Sintered fractures in the Mono Craters obsidian chips collected from fall deposits from a Plinian explosive volcanic plume. Photo credit: J. Gardner. (F) A partially welded tuffisite vein from a bomb at Volcán Chaitén. Photo reproduced with permission from (*52*). (G) Particles of $<5 \times 10^{-5}$ m plastered and sintered in an apparently effusive lava. Photo credit: H. Tuffen.

Second, molten fragments impacting a surface will tend to be captured in a range of regimes [i.e., sticking can occur in the high– or low–Ohnesorge and Weber number regimes (*33*, *34*); see Materials and Methods]. Capture is enhanced by the high angles of impact and the relatively low velocities in the boundary layer at the margins of a turbulent dispersion (*35*), although we do not explicitly model boundary layer processes here. Furthermore, direct experimental evidence shows that an aggrading layer can accumulate when viscous volcanic particles impact a solid surface (*36*).

Third, the time scale for sintering to a low-porosity, dense liquid lava is $10^2 < \lambda < 10^4$ s for the small particles that degas (see Materials and Methods), which is much shorter than the time scale over which lavas are extruded at Earth's surface (*37*). The end result of sintering of crystal-poor rhyolite volcanic ash particles is a dense melt, nearly indistinguishable from magma that was never fragmented, except for the low water content. The equilibrium porosity resulting from complete welding at these conditions is ~3 vol % (*23*), consistent with the range of <5 vol % found in rhyolite lavas (*20*) and without the requirement for repressurization. The cryptic fragmentation model therefore passes the three fundamental feasibility tests.

DISCUSSIONS

Reconciling observations within the cryptic fragmentation model

The model explains an observation that is inconsistent with previous models. The permeable foam and fracture degassing models predict that the effusive products should ascend more slowly than

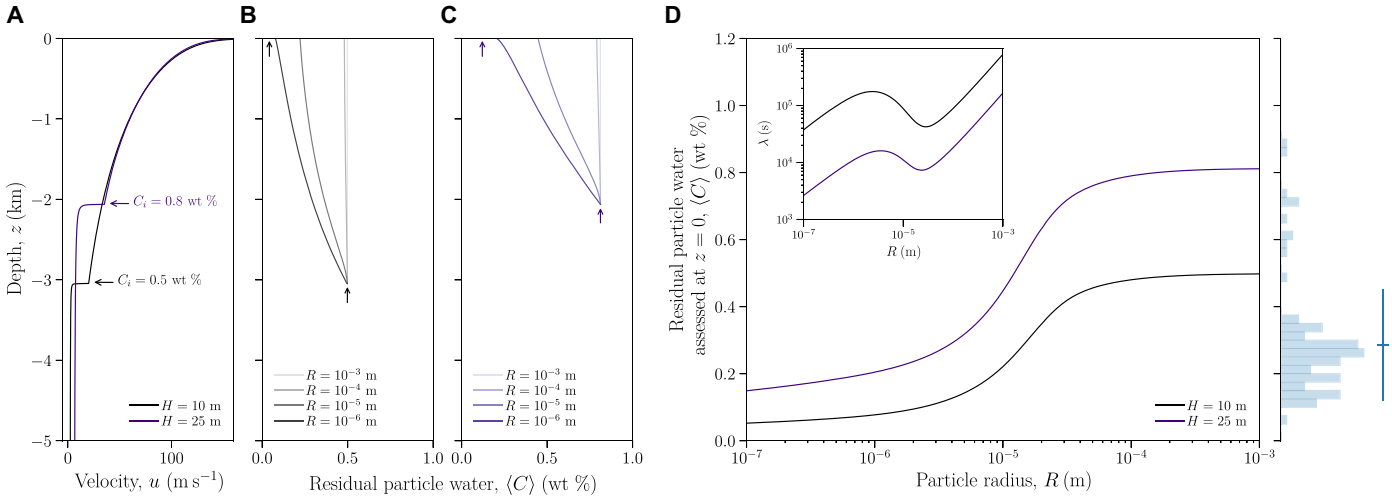

Fig. 3. A quantitative test of the cryptic fragmentation model. (**A**) The output velocity *u* of a magma mixture rising to the surface of Earth, from a one-dimensional volcanic conduit model (*32*) for conduit radii $H = 10$ m and $H = 25$ m. The arrow marks fragmentation (see Fig. 2) and labels the mixture dissolved water content at that point, termed as C_i, which is used to initialize the particle-scale model. (**B** and **C**) The results of the particle-scale model above fragmentation in which the averaged bulk water concentration remnant to a particle $\langle C \rangle$ traveling through the velocity and pressure field toward the surface is tracked [$H = 10$ m (B) and $H = 25$ m (C)] where the upper arrow denotes the equilibrium value at the surface. (**D**) The value of water concentration $\langle C \rangle$ at the point where the particle reaches the surface as a function of the spherical radius of the particle *R*. Large ash particles ($R \gtrsim 10^{-4}$ m) preserve the water concentration at fragmentation and do not equilibrate during eruption, whereas small ash particles ($R \lesssim 10^{-5}$ m) thoroughly degas and are consistent with the mean water concentrations remnant in apparently effusive eruptions (histogram on right axis; see Fig. 1). Inset: the sintering time λ at the surface of Earth for particles with the $\langle C \rangle$ predicted, showing that, once captured, the smallest particles can produce dense lava in under 1 hour; a time scale far shorter than dome extrusion times.

the preceding explosive products. However, analysis of microlite populations in products of the ca. 1460 eruption of the Inyo volcanic chain (*38*) and 2008 eruption of Volcán Chaitén (*1*)—the two rhyolitic eruptions for which reliable estimates of ascent rate are available for both effusive and explosive components—show that the ascent rates overlap (Fig. 4). In our model, both explosively erupted, high-porosity, water-rich pyroclasts and effusively erupted, low-porosity, water-poor lavas may share the same eruptive history up to the shallowest part of the conduit—as part of a gas-ash dispersion. The former does not sinter, while the latter does, but as their divergent passage from the shallowest conduit to surface is too brief to be recorded in microlite populations, both ultimately preserve the evidence for similar average rates of decompression.

Our cryptic fragmentation model also provides a framework for understanding and interpreting recent, detailed, syn-eruptive observations of rhyolitic volcanism, which have demonstrated that apparently effusive events are punctuated by explosive activity and that this type of sustained hybrid behavior may be common (*1*, *2*). The concentration of dissolved volatiles in the products of hybrid activity, such as the partially sintered ash-filled fracture (*28*) shown in Fig. 2F, straddles the range for the explosive and apparently effusive materials (Fig. 1B), supporting the generality of this interpretation. We propose that fracture formation and closing are characteristics of a mature rhyolite eruption, in which much of the shallow conduit has been occluded by aggradation of sintered and outgassed material. In this scenario, the tongue of lava effusing from the vent can be underlain by the gas-and-ash–filled conduit, which periodically "fracks" the lava (Fig. 2C). In addition, the extruding lava is sufficiently degassed that it is highly viscous and therefore prone to shear fracturing at the conduit walls (*9*, *29*, *39*) and tensile failure within domes (*40*). These ash-filled fractures are then advected out of the vent and downflow in the extruded lava, driven by pressure from the gas-ash dispersion (see Materials and Methods). Thus, this model explains the origin of both the gas-ash–rich explosive components of hybrid behavior and the welded textures preserved in apparently effusive lavas.

Further implications

The evolution of particle size distributions produced in large-scale explosive activity plays a central role in determining the evolution of the resultant volcanic hazards. Our model predicts that a proportion of the smallest particles produced at fragmentation degas and stick to conduit walls during eruption. The predicted critical particle radius of ~10^{-5} m (Fig. 3) is consistent with the sizes of particles found incipiently sintered to proximal lava fracture surfaces (Fig. 2G) and with the approximate average size of particles found in moderately welded tuffisite veins (*28*, *31*). An implication is that the total particle size distribution produced at fragmentation is fractionated during transport in the conduit and that the componentry of fall deposits may not record the full distribution, complicating the links between explosivity, fragmentation efficiency, and ash dispersal hazards.

All numerical models for shallow ascent of silicic magma are currently predicated on the assumption that explosive eruptions result when the conditions for fragmentation by bubble overpressure are met, whereas effusive eruptions result when those conditions are not met (*32*). In turn, these models are used to interpret geophysical signals emanating from the shallow subsurface (*41*, *42*) and underpin the starting conditions for models of lava advance or dome behavior. These models, numerical and conceptual, frame the community's conceptions of how we might move toward eruption prediction. However, these models belie the data from rhyolitic eruptions collected over the past few decades and, especially in light of the recent

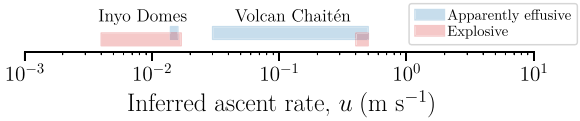

Fig. 4. Ascent rates of subaerial rhyolites recorded by experimental petrology or direct observations of ascent, extrusion, or eruption rates (*38*, *48*, *49*).

observed eruptions, are incomplete. Our cryptic fragmentation model proposes that effusive silicic volcanism is a product of magma fragmentation at depth, such that our model allows all surface activity to be the product of fragmentation at depth. Our model also implies that the transition from explosive to effusive rhyolite activity is a top-down, extrinsic process related to sintering-driven pathway occlusion and not one that is intrinsic to the magma properties or starting conditions. This opens up a new opportunity to build robust, predictive physical models for rhyolite volcanism on Earth. This new generation of models will need to address the potential for nonlinear feedbacks between the position of the fragmentation level, the rate of plug accumulation, and the pressure distribution in the gas-particle dispersion between the two. Coupled modeling of these processes may give a quantitative account of the conditions under which conduit occlusion by sintering of pyroclasts can control the evolution of rhyolitic eruptions from explosive, through hybrid, to effusive, and, ultimately, to cessation.

The analysis that we present focuses on rhyolitic eruptions. However, the discoveries of pervasive healed clastic textures within basaltic phreatomagmatic tephra (*43*), in dome-forming Volcán de Colima of intermediate composition (*44*), and in ash-venting during effusion of lava at Santiaguito volcano (*45*) suggest that cryptic fragmentation may be a more general characteristic of explosive volcanism and not solely confined to the silica-rich end of the magmatic spectrum.

MATERIALS AND METHODS

Database of water contents in rhyolitic glass

We compile a database of dissolved volatile concentration recorded in the glass preserved in either the groundmass of erupted volcanic materials (*10*–*18*, *46*) or inclusions trapped in crystals (*10*–*12*). Materials are identified as effusive, hybrid, or explosive, depending on the description in the work originating the data. The hybrid classification is used for data collected either on bombs erupted explosively (i.e., in an impulsive explosion) but which are interpreted to be pieces of lava that were in the process of being erupted effusively, or on effusive lavas that contain explosive features such as tuffisites. All data from obsidian chips found in fall deposits are classified as explosive. These data are reproduced in Fig. 1. This compilation is not designed to be exhaustive but focusses on data for which both effusive and explosive products were analyzed at sites where the bulk of the material had a substantial glass component and was therefore low crystallinity.

How much magma can fracture-degassing models account for?

The region of the conduit that can be fractured in the fracture-degassing model is confined to the portion of the conduit that experiences strain rates sufficient to induce a brittle magma response to flow. For cylindrical conduits, this region occurs as an annulus at the conduit margins. Following Gonnermann and Manga (*9*), we compute the cross-sectional area fraction of the conduit core that is not involved in this fractured region as $F = (1 - \beta\mu^{0.1})^2$, where μ is the viscosity and β is a coefficient associated with the magma rheology and is 0.01 $(\text{Pa} \cdot \text{s})^{-0.1}$. The higher the value μ takes, the smaller this region will be; therefore, even taking a conservative $\mu = 10^{11}$ Pa·s, we find that $F = 0.76$, implying that only 24% of the cross-sectional area of the conduit can be degassed via fractures.

One-dimensional conduit and diffusion models

We use a versatile one-dimensional, steady-state test bed for volcanic magma ascent problems (*32*). This code solves for the velocity u and pressure P of a magma parcel rising through Earth's crust in a cylindrical conduit of radius H and includes a treatment of magma permeability and outgassing during transport. We use conditions relevant to the 2008 eruption of Volcán Chaitén. These include the conditions of the shallow magma storage region at initial pressure $P_0 = 120$ MPa, depth $Z_0 = 5$ km, zero crystal content (approximately), temperature $T = 800$ ° C, initial water saturated $C_0 = 4.47$ weight % (wt %), and a straight-edged conduit shape of constant radius $H =$ 10 m or $H = 25$ m, values that bracket the observations at Earth's surface [these input values are guided by the experimental campaign of Castro and Dingwell (*1*)]. We input the composition of the erupted glass (*1*), which is used to compute the temperature dependence of the magma viscosity. We use a fragmentation criterion of a consistent critical extensional strain rate of the magma (*50*). In all simulations, the model predicts that the magma fragments within the conduit. We also ran, but do not show results of, simulations with starting water contents equal to the mean values for each of the eruption types shown in Fig. 1A; again, in all simulations, the model predicts that the magma fragments within the conduit. The output of the model is used to (i) find the fragmentation depth and output the water concentration dissolved in the magma at that point, termed C_i, and (ii) compute $u(z)$ and $P(z)$ of the gas-ash-pyroclast dispersion between fragmentation and Earth's surface. We then use a one-dimensional diffusion model to compute the evolution of water concentration in particles of different sizes that track through the velocity and pressure field during transport above fragmentation. This is based on the Fick's equation $\partial C/\partial t = \nabla\cdot(D\nabla C)$, in which D is the temperature- and concentration-dependent diffusivity of water in rhyolite liquids and is given by (*51*). We assume that the boundary of the particles is in equilibrium with output equilibrium C in the gas phase given by the ascent code and that the center of the particles is insulated. This problem is solved using an implicit finite difference scheme for a range of tracer particle radii $10^{-7} < R < 10^{-3}$ m, using tools developed by our group (*52*). We output the average water concentration in the particle $\langle C\rangle$ by integrating across the particle radial profile $C(r)$ as $\langle C\rangle = \int_0^1 C d\bar{r}$, where $\bar{r} = r/R$. The capture of droplets at the wall of the conduit is possible in a range of regimes (high or low Ohnesorge and Weber numbers).

Sintering to form dense effusive lava

For our model to be viable, once captured, there must be sufficient time for the particles to sinter to produce dense lava. The slowest process operative—and therefore the most conservative test of our model—is viscous sintering under the action of surface tension at the interfaces between the captured particles, which acts on time scales $\lambda = R\langle\mu\rangle/\Gamma$, where $\langle\mu\rangle$ is the average viscosity of the particle and Γ is the interfacial tension (0.3 N m^{-1}). The value of λ can be computed by converting $\langle C\rangle$ and T at the surface to $\langle\mu\rangle$ using a viscosity model (*53*).

The result of λ on the order of less than an hour for the most degassed particles (Fig. 3D) is far less than dome extrusion and cooling times of weeks to months (*37*). Any pressure on the droplets in excess of the gas pressure will accelerate this process (*54*, *55*).

Secondary vesiculation

Our model result and the observation of natural, apparently effusive, rhyolite water contents suggest that surficial water can be up to $C \approx 0.2$ wt %. This represents a supersaturation at 1-bar pressure of $\Delta C \approx 0.1$ wt %. Given the long time scales involved in silicic lava emplacement relative to the time scales for degassing into growing bubbles, we can assume that equilibrium water will be reached before the lava cools. Assuming that all the excess water is available for bubble growth, then the pore volume fraction achievable by secondary vesiculation can be calculated from $\phi = \rho\Delta C/(100\,\rho_g + \rho\Delta C)$ where ρ is the melt density and ρ_g is the gas density in the pores. This results in an equilibrium secondary vesiculation of up to 76 vol % porosity. The portions of the captured particles that degas below $C \approx 0.2$, which never decompress to 1 bar or which cool more quickly than bubble growth time scales, remain denser than this value.

Particle size distributions

Our Fig. 2G shows that the particle sizes that have stuck and welded on the incipiently sintered surfaces of fractures in rhyolite lavas are at maximum 10^{-5} m. Particles trapped in tuffisite veins at Panum rhyolite have an approximate mean radius of 2×10^{-5} m measured by x-ray computed tomography (*31*). Those trapped in tuffisite veins at Cordón Caulle (2011–2013) have a mean radius between 5×10^{-6} m and 2×10^{-5} m measured in two dimensions using scanning electron microscopy or estimated using porosimetry (*47*), and those trapped in tuffisites at Volcán Chaitén (2008) have a mean radius approximately 2×10^{-5} m measured using scanning electron microscopy (*28*). These are consistent with the particle size window we predict in our model to be the sizes that can degas and stick in the time available during explosive rhyolite eruptions (Fig. 3) of $\lesssim 10^{-5}$ m.

REFERENCES AND NOTES

1. J. M. Castro, D. B. Dingwell, Rapid ascent of rhyolitic magma at Chaitén Volcano, Chile. *Nature* **461**, 780–783 (2009).
2. C. I. Schipper, J. M. Castro, H. Tuffen, M. R. James, P. How, Shallow vent architecture during hybrid explosive-effusive activity at Cordón Caulle (Chile, 2011-12): Evidence from direct observations and pyroclast textures. *J. Volcanol. Geotherm. Res.* **262**, 25–37 (2013).
3. A. Robock, C. M. Ammann, L. Oman, D. Shindell, S. Levis, G. Stenchikov, Did the Toba volcanic eruption of ~74 ka B.P. produce widespread glaciation? *J. Geophys. Res.* **114**, D10107 (2009).
4. J. H. Fink, S. W. Anderson, in *Encyclopedia of Volcanoes* (Academic Press, 1999), pp. 307–319.
5. M. Cassidy, M. Manga, K. Cashman, O. Bachmann, Controls on explosive-effusive volcanic eruption styles. *Nat. Commun.* **9**, 2839 (2018).
6. J. W. Neuberg, H. Tuffen, L. Collier, D. Green, T. Powell, D. Dingwell, The trigger mechanism of low-frequency earthquakes on Montserrat. *J. Volcanol. Geotherm. Res.* **153**, 37–50 (2006).
7. D. Basualto, P. Pena, C. Delgado, C. Gallegos, H. Moreno, J. O. Munoz, "Seismic activity related to the evolution of the explosive eruption of Chaiten Volcano in the Southern Andes Volcanic Zone," *Am. Geophys. Union, Fall Meet. 2008, Abstr. id. V43D–2178* (2008).
8. C. Jaupart, C. J. Allègre, Gas content, eruption rate and instabilities of eruption regime in silicic volcanoes. *Earth Planet. Sci. Lett.* **102**, 413–429 (1991).
9. H. M. Gonnermann, M. Manga, Explosive volcanism may not be an inevitable consequence of magma fragmentation. *Nature* **426**, 432–435 (2003).
10. J. Owen, H. Tuffen, D. W. McGarvie, Explosive subglacial rhyolitic eruptions in Iceland are fuelled by high magmatic H_2O and closed-system degassing. *Geology* **41**, 251–254 (2013).
11. R. L. Hervig, N. Dunbar, H. R. Westrich, P. R. Kyle, Pre-eruptive water content of rhyolitic magmas as determined by ion microprobe analyses of melt inclusions in phenocrysts. *J. Volcanol. Geotherm. Res.* **36**, 293–302 (1989).
12. K. S. Befus, J. E. Gardner, Magma storage and evolution of the most recent effusive and explosive eruptions from Yellowstone Caldera. *Contrib. Miner. Petrol.* **171**, 30 (2016).
13. B. E. Taylor, J. C. Eichelberger, H. R. Westrich, Hydrogen isotopic evidence of rhyolitic magma degassing during shallow intrusion and eruption. *Nature* **306**, 541–545 (1983).
14. S. Newman, S. Epstein, E. Stolper, Water, carbon dioxide, and hydrogen isotopes in glasses from the ca. 1340 A.D. eruption of the Mono Craters, California: Constraints on degassing phenomena and initial volatile content. *J. Volcanol. Geotherm. Res.* **35**, 75–96 (1988).
15. J. M. Watkins, J. E. Gardner, K. S. Befus, Nonequilibrium degassing, regassing, and vapor fluxing in magmatic feeder systems. *Geology* **45**, 183–186 (2017).
16. J. D. Barnes, T. J. Prather, M. Cisneros, K. Befus, J. E. Gardner, T. E. Larson, Stable chlorine isotope behavior during volcanic degassing of H_2O and CO_2 at Mono Craters, CA. *Bull. Volcanol.* **76**, 805 (2014).
17. J. M. Castro, B. Cordonnier, H. Tuffen, M. J. Tobin, L. Puskar, M. C. Martin, H. A. Bechtel, The role of melt-fracture degassing in defusing explosive rhyolite eruptions at volcán Chaitén. *Earth Planet. Sci. Lett.* **333**, 63–69 (2012).
18. J. M. Castro, I. N. Bindeman, H. Tuffen, C. Ian Schipper, Explosive origin of silicic lava: Textural and δD-H_2O evidence for pyroclastic degassing during rhyolite effusion. *Earth Planet. Sci. Lett.* **405**, 52–61 (2014).
19. J. E. Gardner, E. W. Llewellin, J. M. Watkins, K. S. Befus, Formation of obsidian pyroclasts by sintering of ash particles in the volcanic conduit. *Earth Planet. Sci. Lett.* **459**, 252–263 (2017).
20. J. C. Eichelberger, C. R. Carrigan, H. R. Westrich, R. H. Price, Non-explosive silicic volcanism. *Nature* **323**, 598–602 (1986).
21. H. R. Westrich, J. C. Eichelberger, Gas transport and bubble collapse in rhyolitic magma: An experimental approach. *Bull. Volcanol.* **56**, 447–458 (1994).
22. H. M. Gonnermann, T. Giachetti, C. Fliedner, C. T. Nguyen, B. F. Houghton, J. A. Crozier, R. J. Carey, Permeability during magma expansion and compaction. *J. Geophys. Res. Solid Earth* **122**, 9825–9848 (2017).
23. J. Vasseur, F. B. Wadsworth, Sphere models for pore geometry and fluid permeability in heterogeneous magmas. *Bull. Volcanol.* **79**, 77 (2017).
24. S. Okumura, M. Nakamura, A. Tsuchiyama, T. Nakano, K. Uesugi, Evolution of bubble microstructure in sheared rhyolite: Formation of a channel-like bubble network. *J. Geophys. Res. Solid Earth* **113**, B07208 (2008).
25. A. Cabrera, R. F. Weinberg, H. M. N. Wright, S. Zlotnik, R. A. F. Cas, Melt fracturing and healing: A mechanism for degassing and origin of silicic obsidian. *Geology* **39**, 67–70 (2011).
26. H. Tuffen, D. Dingwell, Fault textures in volcanic conduits: Evidence for seismic trigger mechanisms during silicic eruptions. *Bull. Volcanol.* **67**, 370–387 (2005).
27. G. Macedonio, F. Dobran, A. N.-E. and planetary science letters, undefined 1994, Erosion processes in volcanic conduits and application to the AD 79 eruption of Vesuvius. Elsevier (available at https://www.sciencedirect.com/science/article/pii/0012821X9490037X).
28. E. Saubin, H. Tuffen, L. Gurioli, J. Owen, J. M. Castro, K. Berlo, E. M. McGowan, C. I. Schipper, K. Wehbe, Conduit Dynamics in Transitional Rhyolitic Activity Recorded by Tuffisite Vein Textures from the 2008–2009 Chaitén Eruption. *Front. Earth Sci.* **4**, (2016), doi:10.3389/feart.2016.00059.
29. H. Tuffen, D. B. Dingwell, H. Pinkerton, Repeated fracture and healing of silicic magma generate flow banding and earthquakes? *Geology* **31**, 1089–1092 (2003).
30. M. V. Stasiuk, J. Barclay, M. R. Carroll, C. Jaupart, J. C. Ratté, R. S. J. Sparks, S. R. Tait, Degassing during magma ascent in the Mule Creek vent (USA). *Bull. Volcanol.* **58**, 117–130 (1996).
31. B. A. Black, M. Manga, B. Andrews, Ash production and dispersal from sustained low-intensity Mono-Inyo eruptions. *Bull. Volcanol.* **78**, 57 (2016).
32. W. Degruyter, O. Bachmann, A. Burgisser, M. Manga, The effects of outgassing on the transition between effusive and explosive silicic eruptions. *Earth Planet. Sci. Lett.* **349**, 161–170 (2012).
33. S. Schiaffino, A. A. Sonin, Molten droplet deposition and solidification at low Weber numbers. *Phys. Fluids* **9**, 3172–3187 (1997).
34. C. Josserand, S. T. Thoroddsen, Drop impact on a solid surface. *Rev. Fluid Mech.* **48**, 365–391 (2016).
35. C. Marchioli, A. Soldati, Mechanisms for particle transfer and segregation in a turbulent boundary layer. *J. Fluid Mech.* **468**, 283–315 (2002).
36. C. Giehl, R. Brooker, H. Marxer, M. Nowak, An experimental simulation of volcanic ash deposition in gas turbines and implications for jet engine safety. *Chem. Geol.* (2016) (available at http://www.sciencedirect.com/science/article/pii/S0009254116306258).
37. J. S. Pallister, A. K. Diefenbach, W. C. Burton, J. Muñoz, J. P. Griswold, L. E. Lara, J. B. Lowenstern, C. E. Valenzuela, The Chaitén rhyolite lava dome: Eruption sequence, lava dome volumes, rapid effusion rates and source of the rhyolite magma. *Andean Geol.* **40**, (2013), doi:10.5027/andgeoV40n2-a06.

38. J. M. Castro, J. E. Gardner, Did magma ascent rate control the explosive-effusive transition at the Inyo volcanic chain, California? *Geology* **36**, 279–282 (2008).
39. F. B. Wadsworth, T. Witcher, C. E. J. Vossen, K. U. Hess, H. E. Unwin, B. Scheu, J. M. Castro, D. B. Dingwell, Combined effusive-explosive silicic volcanism straddles the multiphase viscous-to-brittle transition. *Nat. Commun.* **9**, 4696 (2018), doi:10.1038/s41467-018-07187-w.
40. S. W. Anderson, J. H. Fink, Crease structures: Indicators of emplacement rates and surface stress regimes of lava flows. *Geol. Soc. Am. Bull.* **104**, 615–625 (1992).
41. M. E. Thomas, J. Neuberg, What makes a volcano tick-A first explanation of deep multiple seismic sources in ascending magma. *Geology* **40**, 351–354 (2012).
42. A. Goto, A new model for volcanic earthquake at Unzen Volcano: Melt rupture model. *Geophys. Res. Lett.* **26**, 2541–2544 (1999).
43. J. Owen, T. Shea, H. Tuffen, Basalt, unveiling fluid-filled fractures, inducing sediment intra-void transport, ephemerally: Examples from Katla 1918. *J. Volcanol. Geotherm. Res.* **369**, 121–144 (2019).
44. J. E. Kendrick, Y. Lavallée, N. R. Varley, F. B. Wadsworth, O. D. Lamb, J. Vasseur, Blowing off steam: Tuffisite formation as a regulator for lava dome eruptions. *Front. Earth Sci.* **4**, 41 (2016).
45. J. B. Johnson, J. M. Lees, A. Gerst, D. Sahagian, N. Varley, Long-period earthquakes and co-eruptive dome inflation seen with particle image velocimetry. *Nature* **456**, 377–381 (2008).
46. H. Tuffen, J. M. Castro, The emplacement of an obsidian dyke through thin ice: Hrafntinnuhryggur, Krafla Iceland. *J. Volcanol. Geotherm. Res.* **185**, 352–366 (2009).
47. M. J. Heap, H. Tuffen, F. B. Wadsworth, T. Reuschlé, J. M. Castro, C. I. Schipper, The permeability evolution of tuffisites and implications for outgassing through dense rhyolitic magma. *J. Geophys. Res. Solid Earth* **124**, 8281–8299 (2019).
48. B. Browne, L. Szramek, Rates of Magma Ascent and Storage. *Encycl. Volcanoes*, 203–214 (2015).
49. J. M. Castro, C. I. Schipper, S. P. Mueller, A. S. Militzer, A. Amigo, C. S. Parejas, D. Jacob, Storage and eruption of ner-liquidus rhyolite magma at Condon Caulle, Chile. *Bull. Volcanol.* **75**, 702 (2013).
50. P. Papale, Strain-induced magma fragmentation in explosive eruptions. *Nature* **397**, 425–428 (1999).
51. Y. Zhang, H. Ni, Diffusion of H, C, and O components in silicate melts. *Rev. Mineral. Geochem.* **72**, 171–225 (2010).
52. F. B. Wadsworth, J. Vasseur, E. W. Llewellin, K. Genareau, C. Cimarelli, D. B. Dingwell, Size limits for rounding of volcanic ash particles heated by lightning. *J. Geophys. Res. Solid Earth* **122**, 1977–1989 (2017).
53. K. U. Hess, D. B. Dingwell, Viscosities of hydrous leucogranitic melts: A non-Arrhenian model. *Am. Mineral.* **81**, 1297–1300 (1996).
54. F. B. Wadsworth, J. Vasseur, E. W. Llewellin, J. Schauroth, K. J. Dobson, B. Scheu, D. B. Dingwell, Sintering of viscous droplets under surface tension. *Proc. R. Soc. A Math. Phys. Eng. Sci.* **472**, 20150780 (2016).
55. F. B. Wadsworth, J. Vasseur, J. Schauroth, E. W. Llewellin, K. J. Dobson, T. Havard, B. Scheu, F. W. von Aulock, J. E. Gardner, D. B. Dingwell, K.-U. Hess, M. Colombier, F. Marone, H. Tuffen, M. J. Heap, A general model for welding of ash particles in volcanic systems validated using in situ X-ray tomography. *Earth Planet. Sci. Lett.* **525**, 115726 (2019).

Acknowledgments: We thank W. Degruyter for providing the conduit model (*32*) and J. Castro, J. Watkins, and C.I. Schipper for discussion in and out of the field. We thank the Institute for Advanced Studies, Durham University and the Centre for Advanced Study, Ludwig-Maximilians-Universität. **Funding:** This work was funded by NSF via grant EAR-1725186 (to J.E.G.), the U.K. Natural Environment Research Council via grant NE/N002954/1 (to E.W.L.), a Royal University University Research Fellowship (to H.T.), and the European Research Council (ERC) Advanced Grant "Experimental access to volcanic eruptions: Driving observational potential" (EAVESDROP #834225). **Author contributions:** F.B.W., E.W.L., and J.E.G. conceptualized the study. J.V. assisted with numerical analysis. and H.T. provided additional information on recent eruptions. All authors contributed to the manuscript. **Competing interests:** The authors declare that they have no competing interests. **Data and materials availability:** All data needed to evaluate the conclusions in the paper are present in the paper, published references, and/or the Supplementary Materials. Additional data related to this paper may be requested from the authors.

Submitted 6 January 2020
Accepted 22 July 2020
Published 23 September 2020
10.1126/sciadv.aba7940

Citation: F. B. Wadsworth, E. W. Llewellin, J. Vasseur, J. E. Gardner, H. Tuffen, Explosive-effusive volcanic eruption transitions caused by sintering. *Sci. Adv.* **6**, eaba7940 (2020).

Explosive-effusive volcanic eruption transitions caused by sintering

Fabian B. WadsworthEdward W. LlewellinJérémie VasseurJames E. GardnerHugh Tuffen

Sci. Adv., 6 (39), eaba7940.